Graphene Fabry-Perot Cavity Leaky-Wave Antennas: Plasmonic vs. Non-plasmonic Solutions

Walter Fuscaldo, *Student Member, IEEE,* Paolo Burghignoli, *Senior Member, IEEE,*
Paolo Baccarelli, *Member, IEEE,* and Alessandro Galli, *Member, IEEE*

***Abstract*—Tunable THz antennas based on a single unpatterned graphene sheet placed inside a grounded dielectric multilayer are studied with the aim of characterizing their performance in terms of pattern reconfigurability, directivity, and radiation efficiency. The considered structures belong to the class of Fabry-Perot cavity (FPC) antennas, whose radiation mechanism relies on the excitation of cylindrical leaky waves with an ordinary (i.e., non-plasmonic) sinusoidal transverse modal profile. This allows for achieving radiation efficiencies considerably higher than those of alternative graphene-based radiators based on the excitation of surface-plasmon polaritons (SPPs) either in bound or leaky propagation regimes. A customized efficient circuit model has been employed in order to obtain all the radiation characteristics of such graphene FPC antennas, which have been also fully validated by means of a CAD tool. The role of the graphene quality is explicitly taken into account in this comprehensive investigation, proving that it plays a remarkable role in establishing the antenna performance. In particular, it is expected that the standard quality of graphene allows for designing low-efficiency reconfigurable THz antennas based on SPPs and, conversely, high-efficiency FPC antennas with slightly reduced reconfigurability.**

***Index Terms*—Graphene, Leaky-wave antennas, Plasmonics, Fabry-Perot cavities, Terahertz, Tunable antennas.**

I. Introduction

IN THE last decades, the scientific research community has made big efforts in order to close as much as possible the THz gap [1], [2] in view of the number of potential applications with high social and scientific impact [3]–[5]. In this framework, a crucial role is played by the development of efficient and directive THz antennas and sensors [5]–[7].

Graphene [8] is an outstanding material for THz frequencies thanks to its unique electronic properties in this part of the spectrum [9]. Amongst them, the possibility to tune its surface conductivity by the simple application of a bias voltage [8], combined with the possibility of supporting transversely confined surface-plasmon polaritons (SPPs) [10], has opened very interesting perspectives in the context of THz antennas [6], [7]. Recently, the propagation of SPPs along a graphene sheet has been exploited in order to design reconfigurable THz reflectarrays [11], periodic leaky-wave antennas [12], [13], and dipole-like antennas [7]. These devices are able to achieve good performance if compared with the current state of the art in THz antennas [1]. However, the well-known relatively-high losses experienced by SPPs over graphene limit the efficiencies of these antennas to values on the order of 20% [7], [13], [14].

In a previous work [15], starting from the original investigations of Hanson [16], [17], the Authors studied the propagation of leaky waves in a Fabry-Perot Cavity Leaky-Wave Antenna (FPC-LWA) [18]. An alternative FPC-LWA was recently proposed in [19]. However, the directivity of both the antennas in [15] and [19] is rather low. A possible solution for improving the directivity at broadside of the FPC-LWA in [15] has recently been considered by the Authors in [20], where a cover layer (superstrate) is added on the top of the graphene sheet, as suggested in [21] and [22] for designing conventional high-gain printed antennas. As shown in [20], it is possible to further improve the directivity of the antenna by placing the graphene sheet in a suitable position *inside* the substrate. Such a preliminary analysis furnished an *optimum* position in terms of directivity at broadside, but it did not provide any insights about other relevant figures of merit, such as the radiation efficiency and the pattern reconfigurability.

As a matter of fact, it has recently been shown [23], [24] that fundamental limits exist on the efficiency of any reconfigurable graphene antenna. However, we note that the fundamental role of the graphene losses in affecting the performance of such kind of radiators has not been yet properly analyzed in detail. Radiative losses in the class of composite right/left-handed (CRLH) graphene LWAs have been recently considered in [26]. However, a thorough investigation of dissipation losses and radiation efficiencies of THz graphene antennas based both on plasmonic and non-plasmonic field configurations has never been considered in the literature.

In this paper we therefore aim to perform an accurate analysis of the radiative performance in terms of directivity, pattern reconfigurability, and radiation efficiency of graphene-based FPC antennas: we focus our investigation on FPC-LWAs, whose radiation mechanism is based on the excitation of *ordinary* (i.e., non-plasmonic) leaky waves which exhibit a sinusoidal transverse modal profile [15], [20], and compare them with those of graphene antennas based on the excitation of SPPs either in bound or leaky propagation regimes [7], [12], [13] (a few preliminary results of such a study were presented in [25]). The ultimate goal is to assess the true limitations of these devices and ascertain the benefits of designing graphene THz antennas whose radiation mechanism is based on non-plasmonic leaky waves. Furthermore, the role of graphene quality (primarily determined by its relaxation time) has been

Manuscript received Sep. 28, 2016

W. Fuscaldo is with the Department of Information Engineering, Electronics and Telecommunications (DIET), Sapienza University of Rome, 00184 Rome, Italy and with the Institut d'Électronique et de Télécommunications de Rennes (IETR), UMR CNRS 6164, Université de Rennes 1, 35042 Rennes, France (email: fuscaldo@diet.uniroma1.it).

P. Burghignoli, P. Baccarelli, and A. Galli are with the DIET, Sapienza University of Rome, 00184 Rome, Italy.

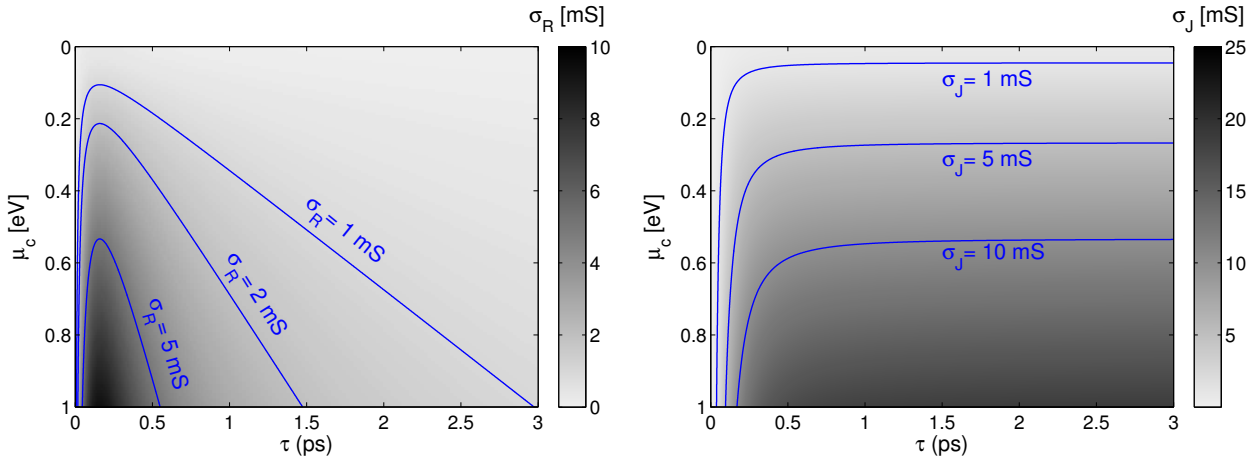

(a) (b)

Fig. 1. (a) Graphene conductance σ_R and (b) graphene susceptance σ_J as a function of the chemical potential μ_c (in the range 0 eV to 1 eV) and of the relaxation time τ (in the range 0 ps to 3 ps) at $f = 1$ THz. σ_J is hereby defined as $-\Im[\sigma]$ due to the inductive nature of graphene in the considered range. Several contour lines are reported in cyan color for both σ_R and σ_J.

carefully addressed, showing how it affects the performance of the proposed devices. Finally, a design trade-off between efficiency, directivity, and angular reconfigurability of the radiation pattern is illustrated for the substrate-superstrate configuration (see, e.g., [20]), which is shown to provide additional desirable degrees of freedom with respect to other solutions [7], [12], [13], [15].

The paper is organized as follows. The role of graphene ohmic losses on plasmonic propagation is analyzed in Sec. II, deriving a simple but rigorous formula. Sec. III is devoted to the analysis of both single- and double-layer graphene FPC-LWAs, whose radiation features are calculated through an ad-hoc circuit model and validated with a commercial CAD software: a comprehensive discussion on efficiency, directivity, and reconfigurability of these antennas is carried out in terms of the available design parameters. Sec. IV discusses important technological issues to be considered in the practical implementation of any graphene-based LWAs. Sec. V provides concluding remarks.

II. Analysis of Losses along Suspended Graphene Sheets

A. Graphene ohmic losses

As is known, graphene is a one-atom thick layer of carbon atoms arranged in a honeycomb lattice. Due to its infinitesimal thickness, graphene is adequately treated as a two-dimensional metamaterial (metasurface) [27] whose surface conductivity is a scalar that can be calculated in the frequency domain through the well-known Kubo formula (neglecting non-local effects) [28]. In particular, in the low THz range, i.e., for $f \in [0.3, 1]$ THz and at room temperature, i.e., $T = 300$ K, the graphene surface conductivity σ is sufficiently well-described by a Drude-like expression by retaining only the intraband contribution of Kubo formula [16], which expresses σ as a complex-valued scalar function of the chemical potential μ_c, the frequency f, and the relaxation time τ:

$$\sigma = \sigma_R - j\sigma_J = \frac{2q_e^2 k_B T}{(\tau^{-1} + j\omega)\pi\hbar^2} \ln\left[\cosh\left(\frac{\mu_c}{2k_B T}\right)\right] \quad (1)$$

where $\omega = 2\pi f$ is the angular frequency (a time dependence $\exp(j\omega t)$ is assumed throughout the paper), q_e is the electron charge, k_B is the Boltzmann constant, and $\hbar$ is the reduced Planck constant; σ_R and -σ_J expressed in Siemens (S) are the conductance and the susceptance of graphene equivalent admittance, respectively. Clearly, when the frequency f is fixed, σ depends only on μ_c and τ. The former (μ_c) usually assumes values from 0 eV to 1 eV [17]. The latter (τ) mainly depends on the quality of the graphene sample; in the current literature various values in the range $0.01 - 10$ ps have been assumed [29].

It is worth here to stress that, despite the existence of sophisticated models [30], [31] which account for the impact of phonon-scattering, grain boundaries and impurities, etc. on graphene quality (either represented by its charge carrier mobility μ, or represented by its relaxation time τ), the latter strongly varies sample by sample, depending also on the adopted synthesis technique [32]. Thus, a thorough analysis of graphene conductivity should take into account the variability of the relaxation time within a suitable range of values provided by experimental data. The interested reader can refer to the recent detailed survey proposed in [33].

In this framework, in order to make our analysis as general as possible, we have considered values of τ ranging from 0 ps to 3 ps (which is the highest value of τ that one can hope for pristine graphene), rather than limit our study to one specific value. In Figs. 1(a) and (b) the values of σ_R and σ_J, at $f = 1$ THz, are reported as functions of τ and μ_c. As expected, the resistive part of graphene conductivity (σ_R) increases as μ_c increases and τ decreases (note that the graphene quality is worse for lower values of τ), whereas its reactive part (σ_J) increases as τ and μ_c both increase. This behavior was already

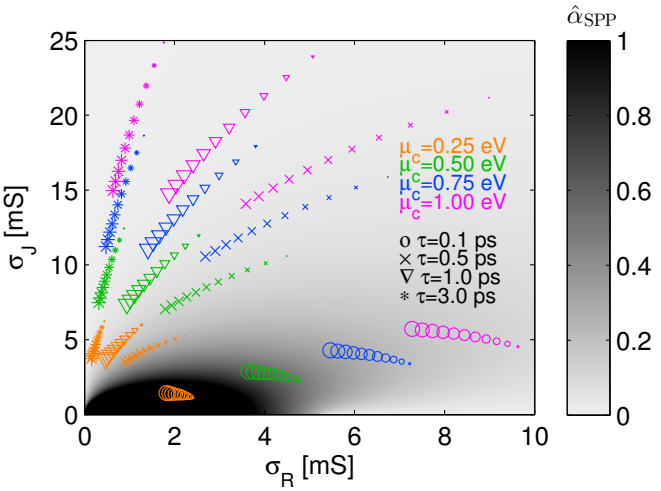

Fig. 2. Intensity of plasmonic dissipation losses $\hat{\alpha}_{\rm SPP}$ in the range $[0,1]$ in the σ complex plane. The dynamic range of $\hat{\alpha}_{\rm SPP}$ has been saturated to values greater than 1 for readability purposes. The paths followed by the graphene surface conductivity in the complex plane have been reported for values of f ranging from 0.75 THz to 1.25 THz (size of the symbols increases), τ ranging from 0.1 ps to 3 ps (symbols change shape in the following order: $\circ, \times, \triangledown, *$) and μ_c ranging from 0.25 eV to 1 eV (color of the symbol change in the following order: orange, green, blue, and magenta). The black region represents the area characterized by the highest dissipation losses and is attained by graphene samples with both lower μ_c and τ.

commented in [15], where it was emphasized that, for high values of μ_c, σ becomes mostly reactive, so that graphene can be switched from a bad to a good conductor when μ_c is raised in the range 0 eV to 1 eV. However, from Fig. 1(a) we now notice that also the ohmic losses increase for high values of μ_c. Hence, biased graphene, even if of good quality (high values of τ), behaves as a good conductor with non-negligible ohmic losses in the considered THz range.

B. Graphene plasmonic losses

As is known [10], a graphene sheet supports an SPP, i.e., an attenuatued surface wave transversely evanescent on both sides of the sheet, with complex wavenumber $\hat{k}_{\rm SPP} = \hat{\beta}_{\rm SPP} - j\hat{\alpha}_{\rm SPP} = k_{\rm SPP}/k_0$ (k_0 being the wavenumber in vacuum). Since $\hat{\beta}_{\rm SPP} \gg 1$, the modal field is highly confined in the vicinity of the sheet.

Both the propagation wavenumber $\hat{k}_{\rm SPP}$ and the modal configuration of the SPP directly depend on σ. For the simplest case of a graphene sheet suspended in vacuum (this is also a good approximation for a graphene sheet in air above a ground plane at a distance greater than half the wavelength in air [12]), $\hat{k}_{\rm SPP}$ can be calculated in closed form [10], [34]. In particular, with the aid of some algebraic manipulations, it is possible to derive an exact formula for the dissipation losses, expressed by $\hat{\alpha}_{\rm SPP}$ as a function of σ_R and σ_J:

$$\hat{\alpha}_{\rm SPP} = -\frac{\sqrt[4]{\Delta^2+\Pi^2}}{\sigma_R^2+\sigma_J^2}\left(\sigma_J\cos\phi_0 + \sigma_R\sin\phi_0\right) \qquad (2)$$

where $\phi_0 = (1/2)\arctan(\Pi/\Delta)$, $\Pi = -2\sigma_R\sigma_J$, and $\Delta = \sigma_R^2 - \sigma_J^2 - 4/\zeta_0^2$ (ζ_0 is the characteristic impedance of vacuum).

In Fig. 2, the value of $\hat{\alpha}_{\rm SPP}$, calculated using Eq. (2), is represented as a greyscale map in the complex plane of σ for the range of values achieved by σ_R and σ_J in Figs. 1(a) and (b), respectively. Furthermore, the paths followed by the σ when frequency ranges from 0.75 THz (the smallest size of the symbols) to 1.25 THz (the largest size of the symbols) are represented for values of μ_c from 0.25 eV to 1 eV (using different colors) and for values of τ from 0.1 ps to 3 ps (using different symbols). Note that $\tau = 0.1$ ps is a typical value for graphene on SiO_2 substrate [26]. It can be observed that:

i) For any biasing status (μ_c) or graphene quality (τ), increasing frequency leads to higher losses (the frequency sensitivity of σ increasing for larger μ_c).
ii) By increasing μ_c, the level of losses decreases (σ moving approximately along a radial line whose slope depends on τ and f).
iii) By increasing τ, the level of losses decreases (σ moving approximately along an arc of circumference centered at the origin whose radius depends on μ_c and f).

Note that we consider here the quantity $\hat{\alpha}_{\rm SPP} = \alpha_{\rm SPP}/k_0 = \alpha_{\rm SPP}\lambda_0/2\pi$ as a figure of merit for the dissipation losses of the SPP since we are dealing with antenna applications, where the relevant dimensions are typically related to the free-space wavelength λ_0. For guided-wave applications (e.g., nano-interconnects, phase shifters, etc.), other figures of merit may be appropriate (such as $\alpha_{\rm SPP}/\beta_{\rm SPP} = \alpha_{\rm SPP}\lambda_g/2\pi$, related to the SPP guided wavelength λ_g)[7], [13], [35].

The operating conditions of most graphene THz antennas based on SPPs found in the literature [7], [12], [13] are such that $\tau \simeq 1$ ps and $\mu_c \simeq 0.5$ eV at frequency of $f \simeq 1$ THz. From Fig. 2, this choice would lead to $\hat{\alpha}_{\rm SPP} \simeq 0.1$ in agreement with the values found in [12], where a silica substrate with $\varepsilon_r = 3.8$ is considered instead of air, (resulting in a scaling factor of $(\varepsilon_r+1)/2$). The resulting dissipation losses are the most important limiting factor for the radiation efficiency η of graphene THz antennas based on SPPs, which are typically lower than 20% [7], [12], [13]. A similar result was recently emphasized in [36] in connection with the use of silver patches in optical nanoantennas. Hence, Eq. (2) as well as Fig. 2 may provide a useful tool for the design of either optical or THz antennas based on metasurfaces (note that Fig. 2 is specifically related to graphene plasmonic losses, but Eq. (2) can be used for any metasurface whose surface admittance σ is known).

III. Analysis of Radiation Efficiencies in FPC-LWAs

In the previous section it has been shown that dissipation losses in SPP-based THz antennas may lead to very low efficiencies. To overcome these limitations, we consider now the propagation of the *ordinary* fundamental TE-TM leaky mode pair inside two different FPC-LWAs: a Graphene-based Single-Layer (GSL) antenna [15] and a Graphene-based Double-Layer (GDL) antenna [20].

Considerable physical insight can be gained by evaluating and comparing the modal field configuration for both the fundamental TM leaky mode and the SPP mode supported

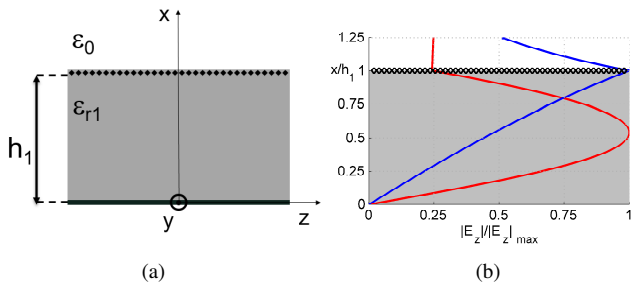

(a) (b)

Fig. 3. (a) Two-dimensional (2-D) sketch of the GSL structure ($\varepsilon_{r1} = 3.8$). The biasing scheme is not reported. (b) Normalized field configurations of the tangential component of the electric field E_z at $f = 0.92$ THz for the fundamental TM leaky mode (red line) and the SPP (blue line) in a GSL antenna. Grey and white regions represent the substrate and the air, respectively, whereas the black diamonds stand for the graphene sheeet. The x-axis is normalized to the height of the substrate h_1.

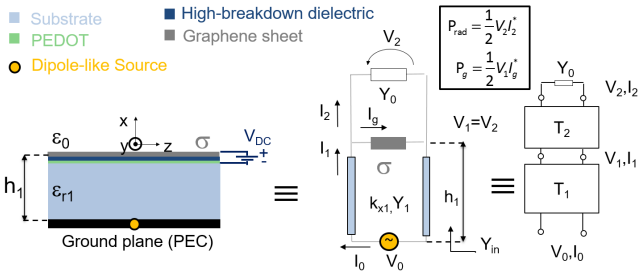

Fig. 4. (2-D) sketch, TEN model, and ABCD-matrix representation of a GSL antenna.

by an FPC-LWA; these have been computed by means of a standard field-matching procedure [37] and are shown in Fig. 3(b) for the GSL structure described in Fig. 3(a) (parameters as in [15]). On one hand, the SPP modal configuration is highly confined in proximity of the graphene sheet where the electric field is maximum. This means that the graphene surface conductivity strongly affects the modal fields and in turn radiation; at the same time, graphene ohmic losses impact more, so that the efficiency is lower. On the other hand, the LW mode configuration resembles the one of the fundamental TM mode of a parallel-plate waveguide (PPW), i.e., an ordinary mode with sinusoidal transverse variation and a maximum on the middle plane of the antenna cavity. As a consequence, the variation of the graphene surface conductivity may have a reduced impact on the radiating features. At the same time, graphene ohmic losses impact less and in turn efficiency should be significantly higher. Such considerations motivate the use of antennas based on *ordinary* leaky waves rather than those based on SPPs (either in guided or leaky regimes), for designing efficient reconfigurable graphene-based THz antennas.

A. Graphene Single-Layer (GSL) Antenna

A GSL antenna [15] (see Fig. 4 with the relevant coordinate frame) consists of a grounded dielectric layer of relative permittivity ε_{r1}, covered with a uniform graphene sheet, possibly biased through the application of an electrostatic field between the graphene sheet and a conductive THz transparent polymer sheet (e.g., PEDOT:PSS [38]) placed just underneath (see Sec. IV for details about the biasing scheme). As in a conventional FPC antenna design [21], the thickness of the dielectric layer h_1 is chosen equal to half the wavelength in the medium at the operating frequency (in all results, parameters $f = 1$ THz, $\varepsilon_{r1} = 3.8$ (SiO_2 layer), and $\tau = 3$ ps, are chosen as in [15]).

In [15], [20] it has been shown that, by exciting the fundamental TE-TM leaky mode pair with a horizontal magnetic dipole (HMD) source placed on the ground plane along y axis, the tunability of graphene conductivity (controlled by an external bias voltage) allows for achieving beam scanning at fixed frequency, which is an uncommon feature for conventional LWAs [18], [39].

With the help of the reciprocity theorem [19], [40], the far-field radiation patterns of the GSL antenna have been calculated based on both the transverse equivalent network (TEN) model shown in Fig. 4 and the electromagnetic CAD tool CST Microwave Studio [41], as in [36]. As is known, for scanned beams the TE leaky mode primarily determines the radiation features in the H-plane (xy-plane), whereas the TM leaky mode determines those in the E-plane (xz-plane) as illustrated in Fig. 5(a); for broadside patterns, both TE and TM leaky modes are required for achieving a directive (pencil) beam [21], [42]. The relevant results for the radiation patterns are reported in Figs. 5(b) and (c) for the H and E planes, respectively. An excellent agreement between our TEN approach and the CAD tool is observed. We finally note that graphene has been modeled in CST with the built-in two-dimensional (2-D) model which implements the full-integral expression of Kubo formula [28]. The almost perfect agreement between our analytical results and full-wave simulations confirms the validity of our approach, in particular as regards the use of Eq.(1) for modeling the graphene surface conductivity, as was also observed in [15], [43] where more sophisticated models taking into account the spatial dispersion of graphene [44] were adopted.

It is important to evaluate the theoretical radiation efficiency in terms of the ratio $\eta = P_{\rm rad}/(P_{\rm rad} + P_{\rm g} + P_L)$ where $P_{\rm rad}$ is the power radiated in space, $P_{\rm g}$ is the power dissipated along the graphene sheet, and P_L is the power dissipated at the antenna termination [45]. As is typical [46], these structures are assumed to be electrically large in the transverse plane so that P_L is negligible, thus η reduces to $\eta = P_{\rm rad}/(P_{\rm rad} + P_{\rm g})$. (Note that practical dimensions of such antennas are on the order of several hundreds of μm as shown in [12], [15]).

The quantities $P_{\rm rad}$ and $P_{\rm g}$ have been evaluated using the TEN model and the ABCD-matrix representation [47] as in Fig. 4, where the ABCD parameters of the transmission matrices T_1 and T_2 are given by: $A_1 = D_1 = \cos(k_{x1}h_1)$, $B_1 = jY_1 \sin(k_{x1}h_1)$, $C_1 = jY_1^{-1} \sin(k_{x1}h_1)$ and $A_2 = D_2 = 1$, $B_2 = 0$, $C_2 = \sigma$, $D_2 = 1$, respectively, where Y_1 and $k_{x1} = \sqrt{(k_0^2\varepsilon_{r1} - k_z^2)}$ are the characteristic admittance and the vertical wavenumber within the substrate, respectively, whereas $k_z = \beta_z - j\alpha_z$ is the complex longitudinal wavenumber, with β_z and α_z the relevant phase and attenuation (or leakage) constants, respectively. Note that k_z and in turn k_x are given by the complex roots of the dispersion equation, obtained by applying the

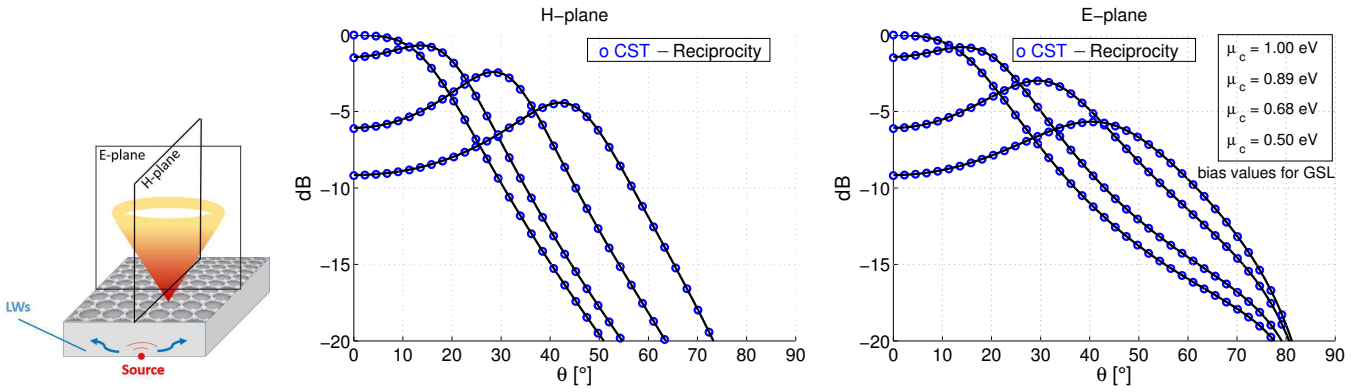

(a) (b) (c)

Fig. 5. (a) Illustrative example of the typical scannable conical beam-scanning feature of a GSL antenna. In (b) and (c), the radiation patterns normalized to the overall maximum (achieved at broadside) vs. elevation angle θ for the GSL antenna represented in (a) are reported for the H-plane and E-plane, respectively. Analytical results are plotted in black solid lines, whereas full-wave results obtained with the tool CST Microwave Studio [41] are given by blue circles. The scanning behavior at a fixed frequency (f_c = 0.922) is shown for beam maxima at $\theta = 0°, 15°, 30°, 45°$. The corresponding chemical potentials are reported in the legend.

transverse resonance technique [15], [47]–[49] on the TEN model in Fig. 4. Here, only the dominant TM-TE leaky modes are considered, thus k_x is selected so that $\Im[k_z] < 0$ and $\Im[k_x] > 0$ [50].

Our analysis shows that for a GSL antenna operating at $f = 0.922$ THz with the fundamental TM leaky mode and pointing at broadside with $\hat{\beta}_z \simeq \hat{\alpha}_z \simeq 0.24$ and $\mu_c = 1$ eV, the theoretical radiation efficiency is $\eta \simeq 70\%$, considerably larger than the values obtained in [7], [12], [13] for graphene-based antennas operating with a SPP. This improved efficiency is paid at the expense of a slightly reduced reconfigurability, as can be seen by comparing the dynamic range of μ_c that is needed to scan an angular range of $45°$ reported in [15] in the case of ordinary leaky waves (there, μ_c scans a range from 1 eV to 0.5 eV)) with the one reported in [12] for SPPs (there, μ_c scans a range from 1 eV to 0.6 eV)).

A concluding remark on the performance of the GSL antenna concerns the obtained directivity. As is seen in Figs. 5(b) and (c), the half-power beamwidth (HPBW) is rather large on both planes, thus directivity is rather low. This is mainly due to the relatively high values attained by the normalized attenuation constant $\hat{\alpha}_z$. To improve directivity, an innovative GDL antenna has recently been proposed in [20]. In the following subsection, we briefly review the main features of such an antenna and discuss, for the first time, its performance in terms of efficiency, directivity, and reconfigurability.

B. Graphene Double-Layer (GDL) Antenna

A GDL antenna [20] (see Fig. 6) consists of a grounded dielectric layer of relative permittivity ε_{r1} (the substrate) in which a graphene sheet is embedded at a suitable position, covered with a dielectric layer of permittivity $\varepsilon_{r2} \gg \varepsilon_{r1}$ (the superstrate). In a conventional substrate-superstrate (SS) antenna [21], directivity at broadside is improved when the thickness of the substrate h_1 and of the superstrate h_2 are chosen equal to a half and to a quarter of the wavelength in the media at the operating frequency, respectively (in all results, parameters $f = 1$ THz, $\varepsilon_{r1} = 3.8$, $\varepsilon_{r2} = 25$, and

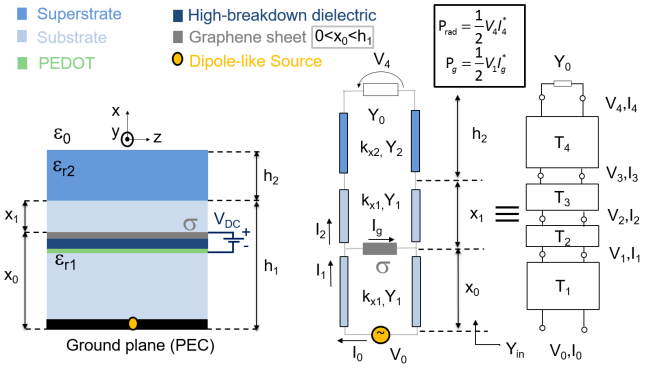

Fig. 6. 2-D sketch, TEN model, and ABCD-matrix representation of a GDL antenna.

$\tau = 3$ ps, are chosen as in [20]). It has recently been shown [20] that when an SS antenna is perturbed by the presence of a graphene monolayer, the directivity at broadside can be further improved if graphene is placed at a suitable position x_0 within the substrate. In [20] a parametric analysis has shown that for $x_0 \simeq 0.8h_1$ the attenuation constant is minimum at the cutoff frequency f_c (i.e., at the frequency for which $\hat{\beta}_z(f_c) = \hat{\alpha}_z(f_c)$ [42]) and hence directivity at broadside is maximum.

It is worth here to remark that in 2-D LWAs the directivity is straightforwardly related to the normalized attenuation constant $\hat{\alpha}_z$. In particular, for directive antennas the half-power beamwidth $\Delta\theta_{\rm BW}$ is given by $\Delta\theta_{\rm BW} \simeq 2\hat{\alpha}_z/\cos\theta$ for $\theta \neq 0$ and $\Delta\theta_{\rm BW} \simeq 2\sqrt{2}\hat{\alpha}_z$ for $\theta = 0$ [46]. Thus, the directivity at broadside ($\theta = 0$) can be approximated by the following formula $D_0 \simeq 4\pi/\Delta\theta^2_{\rm BW} \simeq 0.5\pi/\hat{\alpha}^2_z$.

The radiation patterns of the GDL antenna (Fig. 7(a)) in both the H- and E-planes are reported in Figs. 7(b) and (c), respectively. A comparison of Figs. 5(b) and (c) with Figs. 7(b) and (c) confirms that this *optimized* GDL antenna shows substantially improved directivities with respect to the GSL antenna in the considered angular ranges, as already

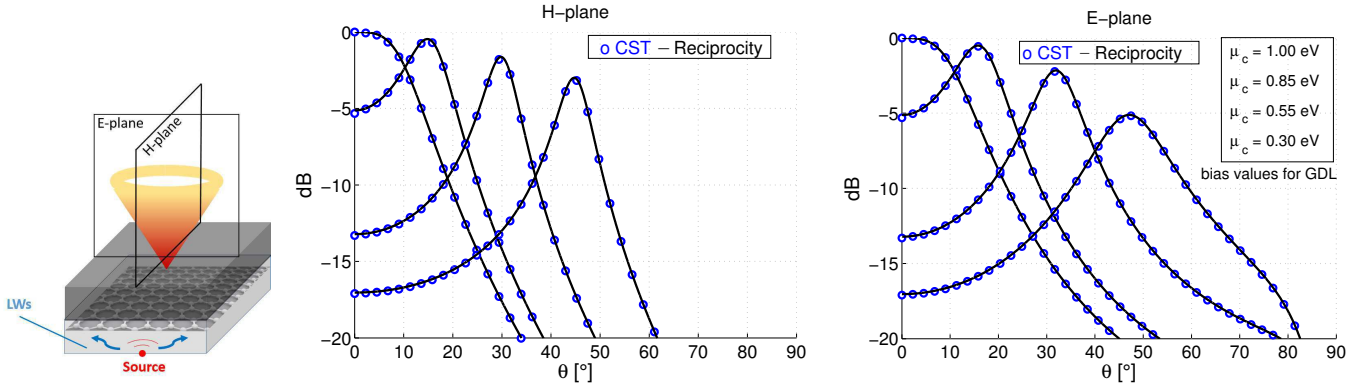

(a) (b) (c)

Fig. 7. (a) Illustrative example of the typical conical beam-scanning feature of a GDL antenna. In (b) and (c), the radiation patterns normalized to the overall maximum (achieved at broadside) vs. elevation angle θ for the GDL antenna represented in (a) are reported for the H-plane and E-plane, respectively. Analytical results are plotted in black solid lines, while full-wave results obtained with the tool CST Microwave Studio [41] are given by blue circles. The scanning behavior at a fixed frequency (f_c = 1.13 THz) is shown for beam maxima at $\theta = 0°, 15°, 30°, 45°$. The corresponding chemical potentials are reported in the legend.

emphasized in [20].

As for the GSL antenna, it is important to evaluate the theoretical radiation efficiency η of the GDL antenna. Following the same procedure outlined in the previous subsection, $P_{\rm g}$ and $P_{\rm rad}$ have been evaluated using the TEN model and the ABCD-matrix representation as in Fig. 6, where the ABCD parameters of the transmission matrices T_1, T_2, T_3, and T_4 are given by: $A_1 = D_1 = \cos(k_{x1}x_0)$, $B_1 = jY_1\sin(k_{x1}x_0)$, $C_1 = jY_1^{-1}\sin(k_{x1}x_0)$, $A_2 = D_2 = 1$, $B_2 = 0$, $C_2 = \sigma$, $A_3 = D_3 = \cos(k_{x1}x_1)$, $B_3 = jY_1\sin(k_{x1}x_1)$, $C_3 = jY_1^{-1}\sin(k_{x1}x_1)$, $A_4 = D_4 = \cos(k_{x2}h_2)$, $B_4 = jY_2\sin(k_{x2}h_2)$, $C_4 = jY_2^{-1}\sin(k_{x2}h_2)$, where Y_2 and $k_{x2} = \sqrt{(k_0^2\varepsilon_{r2} - k_z^2)}$ are the characteristic admittance and the vertical wavenumber within the superstrate, respectively.

In [20] it was shown that the directivity at broadside is a non-linear function of the graphene position x_0. As it can be inferred from the expressions of the ABCD parameters, η is also a non-linear function of the graphene position x_0; this can be observed in Fig. 8, where the values of the efficiency η (thick red solid line) and of the directivity at broadside (thin blue solid line) normalized to its maximum $\bar{D}_0 = D_0/D_{0\max}$ are reported for graphene positions ranging from the ground plane ($x_0 = 0$) to the substrate-superstrate interface ($x_0 = h_1$). Since the maximum directivity does not correspond to a maximum of the efficiency, the *optimal* position for the directivity, i.e., $x_0 = 0.82h_1$, does not lead to the best configuration in terms of efficiency.

In order to take into account both the directivity and the radiation efficiency in the design process of such LWAs, we have therefore defined a suitable function:

$$f(x_0/h_1) = w(\eta(x_0/h_1)) + (1-w)\bar{D}_0(x_0/h_1) \qquad (3)$$

where $w \in [0,1] \subset \mathbb{R}$ is an arbitrary parameter which represents the weight given to the efficiency. Note that $f(x_0/h_1)$ is a convex combination of $\eta(x_0/h_1)$ and $\bar{D}_0(x_0/h_1)$ and that maximizing this function would lead to maximizing the efficiency for $w \to 1$ or to maximizing the directivity at broadside for $w \to 0$. In Fig. 8 the function f is represented for various values of w between 0 and 1. As is seen, the maximum condition (small colored dots in Fig. 8) shifts toward positions x_0 in the proximity of the substrate-superstrate interface (positions too close to the ground plane have not been considered for practical considerations) when w increases; in fact, the efficiency of the GDL antenna is improved when the electric field weakly interacts with the graphene sheet. This physical explanation is also corroborated by the modal configuration of the tangential component of the electric field E_z of the fundamental TM leaky mode in a GDL reported in Fig. 9. As is shown, the intensity of the electric field at the graphene position is stronger when graphene is placed at $x_0 = 0.82h_1$

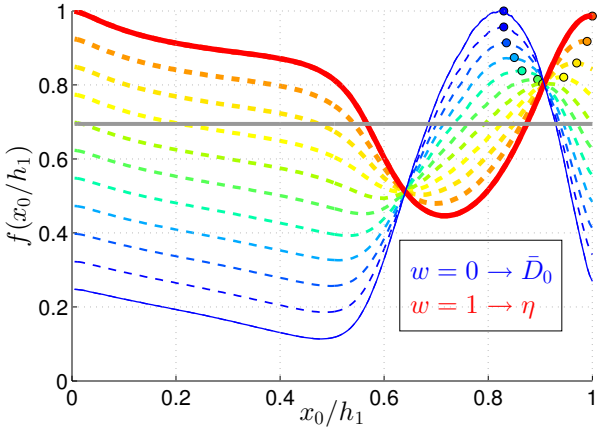

Fig. 8. The function f of Eq. (5) vs. graphene positions in the substrate x_0/h_1 for different values of w. Color (thickness) of the lines shades (increases) from blue to red as w ranges from 0 to 1. For $w = 1$ the efficiency η vs. x_0/h_1 (thick red solid line), and for $w = 0$ directivity at broadside normalized to its maximum $\bar{D}_0$ (thin blue solid line). Both η and $\bar{D}_0$ have been calculated at the corresponding cutoff frequency for each graphene position x_0/h_1. The horizontal grey solid line, representing the efficiency of an equivalent GSL antenna, has been reported for comparison. Colored dots highlight the positions of the maxima of f as w ranges from 0 (blue dot) to 1 (red dot). Maxima are located closer to the interface as the efficiency is weighted more than the directivity.

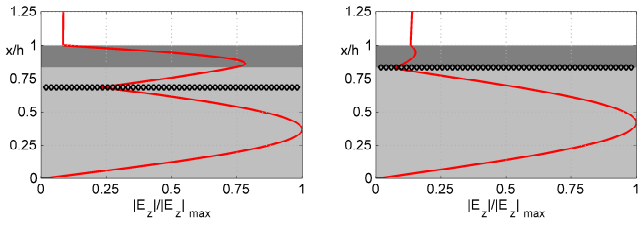

Fig. 9. Field configurations of the tangential component of the electric field E_z for the fundamental TM leaky mode (red line) in a GDL antenna (a) at $f = 1.13$ THz when graphene is placed at $x_0 = 0.82h_1$ and (b) at $f = 1.00$ THz when graphene is placed at the interface $x_0 = h_1$. Light grey, dark grey, and white regions represent the substrate, the superstrate, and the air, respectively, whereas the black diamonds stand for the graphene sheet. The x-axis is normalized to the height of the overall structure $h = h_1 + h_2$.

(see Fig. 9(a)) than when graphene is placed at $x_0 = h_1$ (see Fig. 9(b)). Consequently, the position $x_0 = 0.9h_1$ (see Fig. 8) would lead to both efficiencies η and normalized directivities at broadside $\bar{D}_0$ almost equal to 80% (with the former definitely higher than that of the GSL, see grey solid line in Fig. 8), thus representing a very good trade-off for the antenna design. It is worth noting that this position is correctly predicted by the maximum condition of Eq. (3) when $w = 0.5$ (see small green dot in Fig. 8), i.e., when the same weight is given to η and $\bar{D}_0$ in the maximization of Eq. (3).

Finally, calculations of efficiency and directivity have also been performed considering $\tau = 0.5$ ps and $\tau = 1$ ps in order to show the significant impact of the graphene quality on the performance of both GSL and GDL antennas. The choice of these particular values of τ is motivated by the fact that $\tau = 1$ ps is the value used in [7], [12], [13], whereas $\tau = 0.5$ ps seems to be the best value one can hope to achieve for a graphene flake at room temperature when deposited on impurity-free substrates like SiO_2 [33], [51]. A comparison of the values of efficiency, η, of directivity D_0 in dB, and of reconfigurability, given in terms of the angular range $\Delta\theta$ that can be scanned with a bias variation of 1 eV, is reported in Table I for three different values of τ, namely 0.5 ps, 1 ps and 3 ps, for both the GSL and the GDL antennas, when in the latter x_0/h_1 is chosen to maximize directivity at broadside.

As is shown, the directivity D_0 and the reconfigurability $\Delta\theta$ of both GSL and GDL antennas worsen as the quality of graphene (i.e., τ) decreases. Note that for the GSL antenna the whole angular range from broadside (0°) to endfire (90°) is anyway covered, but with a larger variation of μ_c as τ decreases. However, the efficiency of the GDL antenna counterintuitively improves as τ decreases. This behavior can readily be explained by noting the different positions assumed by the graphene sheet inside the substrate. As it can be seen, when τ decreases, the position which leads the GDL antenna to the configuration that exhibits the maximum directivity at broadside shifts toward the interface where the interaction with the tangential electric field is weaker and thus the efficiency becomes higher. Conversely, the reconfigurability is considerably reduced, as confirmed by the abrupt decrease of $\Delta\theta$ as τ decreases as well. This is mainly due to the fact that, for lower values of τ, graphene ohmic losses are no longer negligible and thus a weaker interaction is preferred for maximizing the directivity, but at the expense of a reduced reconfigurability.

Finally, we have calculated the performance of the GDL antenna when graphene is no longer placed in the position which maximizes directivity at broadside, but in positions that would lead to fixed efficiencies $\eta = 75\%$ and $\eta = 90\%$, respectively. It is worth here to stress that these results are in good agreement with the theoretical limits established in [23] for the efficiency of reconfigurable graphene antennas. Indeed, the theoretical efficiency of a GDL would be upper-bounded by $\eta_{\max} \lesssim 95\%$, as can be inferred looking at the values on the bisector of Fig. 2 in [24] for $\gamma_{\max} = 30$ (the minimum value of $\gamma_{\max}$ for $0.5 < \tau < 3$ ps and $f = 1$ THz, when one considers the maximum achievable angular range, i.e., $\mu_c = 1$ eV and 0 eV is still greater than 70, according to Eq. (10) in [24]). We should also mention that the results of [23], [24] are based on a far-field representation through spherical waves that holds for antennas with finite dimensions [52], in constrast with our initial assumption of transversely-infinite size. However, any practical FPC-LWA is laterally truncated at a suitable radial distance (which depends on both the desired radiation efficiency and the leakage rate, such that the antenna performance is negligibly different from that obtained in the ideal infinite case [15]).

Results are shown in Table II. As expected, a higher efficiency is paid at the expense of a reduced reconfigurability for the aforementioned reasons. In particular, when standard graphene ($\tau = 0.5$ ps) is considered, an extremely efficient GDL antenna ($\eta = 90\%$) would exhibit poor reconfigurable properties, scanning angular regions being limited to an an-

TABLE I
COMPARISON OF EFFICIENCY η, DIRECTIVITY AT BROADSIDE D_0 AND RECONFIGURABILITY $\Delta\theta$ (SCANNING ANGULAR RANGE) FOR GSL AND GDL ANTENNAS, FOR DIFFERENT QUALITY (τ) OF THE GRAPHENE SHEET.

	τ [ps]	x_0/h_1	f_c [THz]	D_0 [dB]	η[%]	$\Delta\theta$ [°]
GSL	3.0	1.000	0.923	14.07	70	90
	1.0	1.000	0.926	12.11	43	90
	0.5	1.000	0.928	10.34	29	90
GDL	3.0	0.820	1.132	18.56	55	70
	1.0	0.910	1.045	16.16	60	37
	0.5	0.940	1.024	14.84	63	28

TABLE II
COMPARISON OF DIRECTIVITY AND RECONFIGURABILITY FOR GDL ANTENNAS WITH DIFFERENT EFFICIENCIES AND FOR DIFFERENT QUALITY (τ) OF THE GRAPHENE SHEET.

	τ [ps]	x_0/h_1	f_c [THz]	D_0 [dB]	$\Delta\theta$ [°]
GDL ($\eta = 75\%$)	3.0	0.890	1.062	17.93	44
	1	0.940	1.023	15.73	28
	0.5	0.955	1.015	14.69	25
GDL ($\eta = 90\%$)	3.0	0.940	1.023	16.48	28
	1.0	0.970	1.007	14.61	21
	0.5	0.980	1.003	13.93	18

gular sector of only 18°. A similar conclusion holds also for LWAs based on SPP as has been stressed in [26] for the graphene CRLH metamaterial waveguides, whose performance is severely affected by the graphene quality. However, our last results emphasize even more the better design flexibility of GDL with respect to GSL antennas, and especially with respect to their counterparts based on SPPs.

IV. Technological aspects

Technological details about the practical realization of the proposed graphene-based LWAs have already been pointed out in [15]. However, the current literature still lacks some useful considerations about the possible implementation of a suitable biasing scheme. As is known [8], the electrostatic field effect allows for tuning the graphene surface conductivity through the simple application of a DC voltage. As shown in [12], [15], [17], an integral equation relates the chemical potential μ_c to the electrostatic field E_0. From Fig. 2 in [17], it is seen that a variation of μ_c in the range 0 to 1 eV requires electrostatic fields of several V/nm. However, the voltage breakdown of the dielectric filling the capacitor constituted by the graphene layer and the conductive polymer layer is rarely taken into account in the literature. Indeed, by means of the approximate formula [53], [54]:

$$E_0 \simeq \frac{q_e}{\varepsilon_0 \varepsilon_r} \frac{1}{\pi} \left(\frac{\mu_c}{\hbar v_{\mathrm{F}}} \right)^2 \tag{4}$$

where $v_{\mathrm{F}} \simeq 10^6$ m/s is the Fermi velocity in graphene, it is easy to find that the maximum chemical potential $\mu_{c,\max}$ that can be achieved for a certain material is given by the formula:

$$\mu_{c,\max} = \hbar v_{\mathrm{F}} \sqrt{\frac{\pi \varepsilon_0 \varepsilon_r E_{\mathrm{bd}}}{q_e}} \tag{5}$$

where E_{bd} represents the voltage breakdown of a given dielectric material. If ones uses E_{bd} of SiO_2 ($\varepsilon_r = 3.8$, $E_{\mathrm{bd}} = 1.5$ V/nm) which is one of the materials with the highest E_{bd} [55], it comes out that the maximum chemical potential that can be achieved is only 0.436 eV. However, since $\mu_{c,\max}$ depends not only on E_{bd} but also on ε_r, an accurate analysis of Table I in [55] revealed us that the choice of HfO_2 ($\varepsilon_r = 25$ and $E_{\mathrm{bd}} = 0.67$ V/nm), TiO_2 ($\varepsilon_r = 95$ and $E_{\mathrm{bd}} = 0.25$ V/nm), and Al_2O_3 ($\varepsilon_r = 9$ and $E_{\mathrm{bd}} = 1.38$ V/nm) lead to values of $\mu_{c,\max}$ equal to 1.12 eV, 1.33eV, and 0.92 eV respectively. It is worth here noting that, even if both HfO_2, TiO_2, and Al_2O_3 are characterized by a non-negligible loss tangent in the THz range [56], [58], the extremely thin layer that is needed in our design would result in a negligible impact on the performance of the antenna. It should also be noted that these materials (viz., HfO_2, TiO_2 and Al_2O_3) provide minimal degradation of epitaxial graphene structural properties when integrated with thin dielectric layers [57]. In particular, it is seen that Al_2O_3 is only mildly affected by surface-optical phonon-scattering with respect to other high-permittivity materials [31]. On the other hand, it has been shown that high-permittivity materials are subject to phonon scattering, which reduces the mobility of graphene [31]. A good choice is represented by Alumina (Al_2O_3).

Furthermore, very recently new techniques involving ion gel gate dielectrics [53], [59] seem to provide an innovative solution in order to bias graphene up to 1 eV avoiding the problems posed by the voltage breakdown of the most common dielectric materials.

As a final comment, since in our design the minimum value of the chemical potential for scanning the beam at 45° is of the order of 0.30 eV [20], a suitable solution in order to avoid the use of TiO_2 and HfO_2 could be represented by the possibility of chemically pre-doping graphene. Note also that chemical doping seems to scarcely affect the mobility of carriers in graphene [8].

V. Conclusion

The analysis of dissipation losses in plasmonic graphene-based THz antennas has shown to lead to very low radiation efficiencies. A different class of radiators, whose mechanism of radiation is based on the propagation of ordinary leaky modes, has thus been considered in detail. In particular, two graphene-based Fabry-Perot cavity leaky-wave antennas have been analyzed in terms of directivity, efficiency, and reconfigurability, using both original and efficient analytical models based on standard field-matching procedures or transverse equivalent networks and full-wave commercial simulation tools.

It has been found that the considered configurations allow for significantly improving the radiation efficiency at the expense of a slightly reduced pattern reconfigurability. In particular, a trade-off is shown to exist between efficiency, directivity, and reconfigurability when designing either plasmonic or non-plasmonic graphene-based THz antennas. A particular non-plasmonic radiator, i.e., the graphene-based double-layer antenna has shown attractive design flexibility considering the typical antenna constraints.

Finally, the impact of graphene quality on the overall performance of Fabry-Perot cavity leaky-wave antennas has been properly addressed, showing that, when standard graphene is considered, a very efficient radiator can still be designed, provided a certain reduction of its tunability is accepted.

Acknowledgments

The authors would like to thank Michele Tamagnone and Juan Sebastián Gómez-Díaz for fruitful discussions on these topics.

References

[1] G. P. Williams, "Filling the THz gap - high power sources and applications," *Rep. Prog. Phys.*, vol. 69, no. 2, pp. 301-326, Dec. 2005.
[2] M. Tonouchi, "Cutting-edge terahertz technology," *Nature Photonics*, vol. 1, no. 2, pp. 97-105, Feb. 2007.
[3] M. C. Kemp et al., "Security applications of terahertz technology," *Proc. SPIE*, vol. 5070, pp. 44-52, Aug. 2003.
[4] E. Pickwell and V. P. Wallace, "Biomedical applications of terahertz technology," *J. Phys. D Appl. Phys.*, vol. 39, no. 17, pp. R301-R310, Aug. 2006.
[5] P. Mukherjee and B. Gupta, "Terahertz (THz) frequency sources and antennas - a brief review," *Int. J. Infrared Milli. Waves*, vol. 29, pp. 1091-1102, Sep. 2008.
[6] J M. Jornet and I. F. Akyildiz, "Graphene-based nano-antennas for electromagnetic nanocommunications in the terahertz band," *4th Eur. Conf. Antennas Propag. (EuCAP, 2010)*, Barcelona, Spain, 12-16 Apr. 2010, pp. 1-5.

[7] M. Tamagnone, J. S. Gómez-Díaz, J. R. Mosig, and J. Perruisseau-Carrier, "Reconfigurable terahertz plasmonic antenna concept using a graphene stack," *App. Phys. Lett.*, vol. 101, 214102, Nov. 2012.

[8] A. K. Geim and K. S. Novoselov, "The rise of graphene," *Nat. Mater.*, vol. 6, pp. 183-191, Mar. 2007.

[9] K. S. Novoselov et al., "A roadmap for graphene," *Nature*, vol. 490, pp. 192-200, Oct. 2012.

[10] A. Vakil and N. Engheta, "Transformation optics using graphene," *Science*, vol. 32, pp. 1291-1294, Jun. 2011.

[11] E. Carrasco and J. Perruisseau-Carrier, "Reflectarray antenna at terahertz using graphene," *IEEE Antennas Wireless Propag. Lett.*, vol. 12, pp. 253-256, Feb. 2013.

[12] M. Esquius-Morote, J. S. Gómez-Díaz, and J. Perruisseau-Carrier, "Sinusoidally modulated graphene leaky-wave antenna for electronic beamscanning at THz," *IEEE Trans. THz Sci. Technol.*, vol. 4, no. 1, pp. 116-122, Jan. 2014.

[13] J. S. Gómez-Díaz, M. Esquius-Morote, and J. Perruisseau-Carrier, "Plane wave excitation-detection of non-resonant plasmons along finite-width graphene strips," *Opt. Express*, vol. 21, no. 21, pp. 24856-24872, Oct. 2013.

[14] D. Correas-Serrano et al., "Electrically and magnetically biased graphene-based cylindrical waveguides: analysis and applications as reconfigurable antennas," *IEEE Trans. THz Sci. Technol.*, vol 5, no. 6, pp. 951-960, Nov. 2015.

[15] W. Fuscaldo, P. Burghignoli, P. Baccarelli, and A. Galli, "Complex mode spectra of graphene-based planar structures for THz applications," *J. Infrared Milli. Terahz Waves*, vol. 36, no. 8, pp. 720-733, Aug. 2015.

[16] G. W. Hanson, "Dyadic Green's functions and guided surface waves for a surface conductivity model of graphene," *J. App. Phys.*, vol. 103, 064302, Mar. 2008.

[17] G. W. Hanson, "Dyadic Green's functions for an anisotropic, non-local model of biased graphene," *IEEE Trans. Antennas Propag.*, vol. 56, no. 3, pp. 747-757, Mar. 2008.

[18] G. Lovat, P. Burghignoli, and S. Celozzi, "A tunable ferroelectric antenna for fixed-frequency scanning applications," *IEEE Antennas Wireless Propag. Lett.*, vol. 5, pp. 353-356, Jun. 2006.

[19] X.-C. Wang, W.-S. Zhao, J. Hu, and W.-Y. Yin, "Reconfigurable terahertz leaky-wave antenna using graphene-based high-impedance surface," *IEEE Trans. Nanotechnol.*, vol. 14, no. 1, pp. 62-69, Jan. 2015.

[20] W. Fuscaldo, P. Burghignoli, P. Baccarelli, and A. Galli, "A reconfigurable substrate-superstrate graphene-based leaky-wave THz antenna," *IEEE Antennas Wireless Propag. Lett.*, vol. 15, pp. 1545-1548, Apr. 2016.

[21] D. R. Jackson and A. A. Oliner, "A leaky-wave analysis of the high-gain printed antenna configuration," *IEEE Trans. Antennas Propag.*, vol. 36, no. 7, pp. 905-910, Jul. 1988.

[22] N. Alexópoulos and D. R. Jackson, "Fundamental superstrate (cover) effects on printed circuit antennas," *IEEE Trans. Antennas Propag.*, vol. 32, no. 8, pp. 807-816, Aug. 1984.

[23] M. Tamagnone, A. Fallahi, J. R. Mosig, and J. Perruisseau-Carrier, "Fundamental limits and near-optimal design of graphene modulators and non-reciprocal devices," *Nat. Photonics*, vol. 8, 10.1038, Jul. 2014.

[24] M. Tamagnone and J. R. Mosig, "Theoretical limits on the efficiency of reconfigurable and nonreciprocal graphene antennas," *IEEE Antennas Wireless Propag. Lett.*, vol. 15, Apr. 2016.

[25] W. Fuscaldo, P. Burghignoli, P. Baccarelli, and A. Galli, "Efficient 2-D leaky-wave antenna configurations based on graphene metasurfaces," *46th Eur. Microw. Conf. (EuMW 2016)*, London, UK, 3-7 Oct. 2016.

[26] D. A. Chu, P. W. C. Hon, T. Itoh, and B. S. Williams, "Feasibility of graphene CRLH metamaterial waveguides and leaky wave antennas," *J. App. Phys.*, vol. 120, 013103, Jul. 2016.

[27] C. L. Holloway et al. "An overview of the theory and applications of metasurfaces: The two-dimensional equivalents of metamaterials," *IEEE Antennas Propag. Magazine*, vol. 54, no. 2, pp. 10-35, Apr. 2012.

[28] V. P. Gusynin, S. G. Sharapov, and J. B. Charbotte, "On the universal AC optical background in graphene," *New J. Phys.*, vol. 11, 095013, Sep. 2009.

[29] I. Llatser et al., "Graphene-based nano-patch antenna for Terahertz radiation," *Phot. Nano. Fund. Appl.*, vol. 10, pp. 353-358, May 2012.

[30] L. A. Ponomarenko et al., "Effect of a high-k environment on charge carrier mobility in graphene," *Phys. Rev. Lett.*, vol. 102, 206603, May 2009.

[31] A. Konar et al., "Effect of high-k gate dielectrics on charge transport in graphene-based field effect transistors," *Phys. Rev. B*, vol. 82, 115452, Sep. 2010.

[32] R. Raccichini, A. Varzi, S. Passerini, and B. Scorsati, "The role of graphene for electrochemical energy storage," *Nat. Mater.*, vol. 14, pp. 271-279, Mar. 2015.

[33] W. Zouaghi et al., "How good would the conductivity of graphene have to be to make single-layer-graphene metamaterials for terahertz frequencies feasible?," *Carbon*, vol. 94, pp. 301-308, Jun. 2015.

[34] S. A. Maier, *Plasmonics: Fundamentals and Applications*, Springer: Science & Business Media, 2007.

[35] P. Berini, "Figures of merit for surface plasmon waveguides," *Opt. Express*, vol. 14, no. 26, pp. 13030-13042, Dec. 2006.

[36] M. Lorente-Crespo and C. Mateo-Segura, "Highly directive Fabry-Perot leaky-wave nanoantennas based on optical partially reflective surfaces," *App. Phys. Lett.*, vol. 106, no. 18, 183104, May 2015.

[37] D. Comite, P. Burghignoli, P. Baccarelli, D. Di Ruscio, and A. Galli, "Equivalent-network analysis of propagation and radiation features in wire-medium loaded planar structures," *IEEE Trans. Antennas Propag.*, vol. 63, no. 12, pp. 5573-5585, Dec. 2015.

[38] M. Vosgueritchian, D.-J. Lipomi, and Z. Bao, "Highly conductive and transparent PEDOT: PSS films with a fluorosurfactant for stretchable and flexible transparent electrodes," *Adv. Functional Materials*, vol. 22, no. 2, pp. 421-428, Nov. 2011.

[39] P. Baccarelli, C. Di Nallo, F. Frezza, A. Galli, and P. Lampariello, "Attractive features of leaky-wave antennas based on ferrite-loaded open waveguides," *IEEE Antennas Propag. Soc. Int. Symp. (IEEE AP-S, 1997)*, Montreal, Quebec, Canada, 1997, pp. 1442-1445.

[40] T. Zhao, D. R. Jackson, J. T. Williams, and A. A. Oliner, "General formulas for 2-D leaky-wave antennas," *IEEE Trans. Antennas Propag.*, vol. 53, no. 11, pp. 3525-3533, Nov. 2005.

[41] CST products, Germany, 2014 [Online]. Available: www.cst.com

[42] G. Lovat, P. Burghignoli, and D. R. Jackson, "Fundamental properties and optimization of broadside radiation from uniform leaky-wave antennas," *IEEE Trans. Antennas Propag.*, vol. 54, no. 5, pp. 1442-1452, May 2006.

[43] W. Fuscaldo, P. Burghignoli, P. Baccarelli, and A. Galli, "Graphene-based reconfigurable leaky-wave antennas for THz applications," *15th Medit. Microw. Symp. (MMS 2015)*, Lecce, Italy, 2015, pp. 1-4.

[44] G. Lovat, G. W. Hanson, R. Araneo, and P. Burghignoli, "Semiclassical spatially dispersive intraband conductivity tensor and quantum capacitance of graphene," *Phys. Rev. B*, vol. 87, no. 11, 115429, Mar. 2013.

[45] C. Di Nallo, F. Frezza, A. Galli, and P. Lampariello, "Rigorous evaluation of ohmic loss effects for accurate design of traveling-wave antennas," *J. Electromagn. Waves Appl.*, vol. 12, no. 1, pp. 39-58, 1998.

[46] D. R. Jackson and A. A. Oliner, "Leaky-Wave Antennas," in *Modern Antenna Handbook*, C. A. Balanis, John Wiley & Sons, 2011.

[47] D. M. Pozar, *Microwave Engineering*. John Wiley & Sons, 2009.

[48] G. Valerio, D. R. Jackson, and A. Galli, "Fundamental properties of surface waves in lossless stratified structures," *Proc. Royal Soc. A*, vol. 446, pp. 2447-2469, Mar. 2010.

[49] R. Sorrentino, *Numerical Techniques for Microwave and Millimeter-wave Passive Structures*, ed. by T. Itoh, John Wiley & Sons, 1989.

[50] T. Tamir and A. A. Oliner, "Guided complex waves. Part I: fields at an interface. Part II: relation to radiation patterns," *Proc. Inst. Elect. Eng.*, vol. 110, no. 2, pp. 310-334, Feb. 1963.

[51] J. -H. Chen et al., "Intrinsic and extrinsic performance limits of graphene devices on SiO2," *Nature Nanotechnol.*, vol. 3, no. 4, pp. 206-209, Mar. 2008.

[52] C. A. Balanis, *Advanced Engineering Electromagnetics*, John Wiley & Sons, 2012.

[53] L. Ju et al., "Graphene plasmonics for tunable terahertz metamaterials," *Nature Nanotechnol.*, vol. 6, no. 10, pp. 630-634, Nov. 2011.

[54] K. S. Novoselov et al., "Two-dimensional gas of massless Dirac fermions in graphene," *Nature*, vol. 438, no. 7065, pp. 197-200, Nov. 2005.

[55] J. W. McPherson et al., "Trends in the ultimate breakdown strength of high dielectric-constant materials," *IEEE Trans. Electron Dev.*, vol. 50, no. 8, pp. 1771-1778, Aug. 2003.

[56] P. Sharma, J. Perruisseau-Carrier, C. Moldovan, and A. Inescu, "Electromagnetic performance of RF NEMS graphene capacitive switches," *IEEE Trans. Nanotechnol.*, vol. 13, no. 1, pp. 70-79, Jan. 2014.

[57] J. A. Robinson et al., "Epitaxial graphene materials integration: effects of dielectric overlayers on structural and electronic properties," *ACS Nano*, vol. 4, no. 5, pp. 2667-2672, Apr. 2010.

[58] K. Berdel et al., "Temperature dependence of the permittivity and loss tangent of high-permittivity materials at terahertz frequencies," *IEEE Trans. Microw. Theory Tech.*, vol. 53, no. 4, pp. 1266-1271, Apr. 2005.

[59] B. J. Kim et al., "High-performance flexible graphene field effect transistors with ion gel gate dielectrics," *Nano Lett.*, vol. 10, no. 9, pp. 3464-3466, Aug. 2010.

Walter Fuscaldo (S'15) was born in Rome, Italy, on May 13, 1987. He received the B.Sc. and M.Sc. (cum laude) degrees in telecommunications engineering from Sapienza University of Rome, Rome, Italy, in 2010 and 2013, respectively. He is currently pursuing the Ph.D. degree in cotutelle agreement between the Department of Information Engineering, Electronics and Telecommunications, Sapienza University of Rome, Rome, Italy and the Institut d'Électronique et de Télécommunications de Rennes (IETR), Université de Rennes 1, France. From September 2014 to December 2014 He was a Visiting Researcher at NATO-STO Centre for Maritime Research and Experimentation (CMRE) in La Spezia, Italy. From May 2016 to September 2016, he was a Visiting Researcher with the University of Houston, Houston, TX. His research interests include propagation of leaky waves, surface waves and surface plasmon polaritons, analysis and design of leaky-wave antennas and millimeter-wave focusing systems, generation of limited-diffraction limited-dispersion electromagnetic pulses, and graphene electromagnetics. Mr. Fuscaldo was the recipient of the Yarman-Carlin Student Award at the IEEE 15th Mediterranean Microwave Symposium (MMS 2015) in 2015, and of the Young Engineer Prize for the best paper presented at the 46th European Microwave Conference (EuMC 2016) in 2016.

Paolo Burghignoli (S'97-M'01-SM'08) was born in Rome, Italy, on February 18, 1973. He received the Laurea degree (cum laude) in Electronic Engineering and the Ph.D. degree in Applied Electromagnetics from Sapienza University of Rome, Rome, Italy, in 1997 and 2001, respectively. In 1997, he joined the Electronic Engineering Department, now Department of Information Engineering, Electronics and Telecommunications, Sapienza University of Rome. From November 2010 to October 2015 he was an Assistant Professor and since November 2015 he has been an Associate Professor in the same University. From January 2004 to July 2004, he was a Visiting Research Assistant Professor with the University of Houston, Houston, TX. His scientific interests include analysis and design of planar antennas and arrays, leakage phenomena in uniform and periodic structures, numerical methods for integral equations and periodic structures, propagation and radiation in metamaterials, and graphene electromagnetics. Dr. Burghignoli was the recipient of the "Giorgio Barzilai" Laurea Prize (1996-1997) presented by the former IEEE Central & South Italy Section, of a 2003 IEEE MTT-S Graduate Fellowship, and of a 2005 Raj Mittra Travel Grant for Junior Researchers presented at the IEEE AP-S Symposium on Antennas and Propagation, Washington, DC. He is a coauthor of the "Fast Breaking Papers, October 2007" in EE and CS, about metamaterials (paper that had the highest percentage increase in citations in Essential Science Indicators, ESI).

Paolo Baccarelli (M'01) received the Laurea degree in electronic engineering and the Ph.D. degree in applied electromagnetics from Sapienza University of Rome, Rome, Italy, in 1996 and 2000, respectively. In 1996 he joined the Department of Electronic Engineering, Sapienza University of Rome, where he is an Assistant Professor since November 2010. From April 1999 to October 1999, he was a Visiting Researcher with the University of Houston, Houston, TX. He has co-authored about 70 international journal papers and book chapters and about 140 international conference contributions. His research interests include analysis and design of planar antennas and arrays, leakage phenomena in uniform and periodic structures, numerical methods for integral equations and periodic structures, propagation and radiation in anisotropic media, metamaterials, graphene, and electromagnetic band-gap structures. Dr. Baccarelli was the recipient of the "Giorgio Barzilai" Laurea Prize (1994-1995) presented by the former IEEE Central & South Italy Section; he is in the editorial board of international journals and acts as reviewer for more than 20 IEEE, IET, OSA, and AGU journals; he was Secretary of the "2009-European Microwave Week" (EuMW 2009) and has been member of the TPCs of several international conferences.

Alessandro Galli (S'91-M'96) received the Laurea degree in Electronic Engineering and the Ph.D. degree in Applied Electromagnetics from Sapienza University of Rome, Italy, in 1990 and 1994, respectively. Since 1990, he has been with the Department of Electronic Engineering (now Department of Information Engineering, Electronics, and Telecommunications) of Sapienza University of Rome. In 2000 he became an Assistant Professor, and in 2002 an Associate Professor at Sapienza University of Rome; in 2013 he passed the National Scientific Qualification as a Full Professor in the sector of Electromagnetics. For the educational activities, he is currently teaching the courses of "Electromagnetic Fields," "Antennas and Propagation," and "Engineering Electromagnetics" for Electronics and Communications Engineering at Sapienza University of Rome. He has authored more than 300 papers on journals, books, and conferences. His research interests include theoretical and applied electromagnetics, mainly focused on modeling, numerical analysis, and design for antennas and passive devices from microwaves to terahertz: specific topics involve leaky waves, periodic and multilayered printed structures, metamaterials, and graphene. Other topics of interest involve geoelectromagnetics, bioelectromagnetics, and microwave plasma heating for alternative energy sources. He is author of a patent for an invention concerning a type of microwave antenna. Dr. Galli was elected as the Italian representative of the Board of Directors of the "European Microwave Association" (EuMA), the main European Society of electromagnetics, for the 2010-2012 triennium and then re-elected for the 2013-2015 triennium. He was the General Co-chair of the "European Microwave Week" (EuMW), the most important conference event in the electromagnetic area at European level in 2014. Since its foundation in 2012, he is the Coordinator of the "European Courses on Microwaves" (EuCoM), the first European educational institution on microwaves. He is also a member of the "European School of Antennas" (ESoA). He is a member of the leading scientific societies of electromagnetics, and an Associate Editor of the "International Journal of Microwave and Wireless Technologies" (Cambridge University Press) and of the "IET Microwaves, Antennas & Propagation" (Institution of Engineering and Technology). He was the recipient of various grants and prizes for his research activity: he won in 1994 the "Barzilai Prize" for the best scientific work of under-35 researchers at the "10th National Meeting of Electromagnetics", and in 1994 and 1995 the "Quality Presentation Recognition Award" at the International Microwave Symposium by the "Microwave Theory and Techniques" (MTT) Society of the Institute of Electrical and Electronics Engineering (IEEE).